Power attenuation of Martian rovers and landers solar panels due to dust deposition

Thomas Pierron, François Forget, Ehouarn Millour, Antoine Bierjon

Planetary and Space Science 253 (2024) 105985

Contents lists available at ScienceDirect

Planetary and Space Science

journal homepage: www.elsevier.com/locate/pss

Power attenuation of Martian rovers and landers solar panels due to dust deposition

Thomas Pierron *, François Forget, Ehouarn Millour, Antoine Bierjon

Laboratoire de Météorologie Dynamique, Institut Pierre-Simon Laplace (LMD/IPSL), Sorbonne Université, Centre National de la Recherche Scientifique (CNRS), École Polytechnique, École Normale Supérieure (ENS), Paris, France

A B S T R A C T

Because of the high amount of dust in the Martian atmosphere, solar panels of landers and rovers on Mars get covered by dust in the course of their mission. This accumulation significantly decreases the available power over sols. During some missions, winds were able to blow the dust away. These "dust cleaning events", as they are called, were followed by an increase of the electrical current produced by the solar arrays. However, the Insight Lander solar panels were never cleaned and the mission died of dust accumulation. In order to better predict the evolution of available power produced by solar panels in the Martian conditions, this paper proposes a model of dust accumulation in which the solar flux under the accumulated dust layer is computed taking into account a full radiative transfer in the atmosphere and in the dust layer accumulated on the panel. This work uses several missions observation data to validate this model.

1. Introduction

Knowing the amount of available electrical power produced by solar panels for future missions on Mars is mandatory to prepare as best as possible the operations. Several studies have already been conduced to model the effect of dust accumulation on solar panels. Some predict the fraction of solar flux reaching the panel and actually producing the electrical current, as it is done in Landis (1996) and Landis and Jenkins (2000), using single scattering theory and assuming a constant dust opacity of the accumulated dust layer to calculate this fraction. Other studies use a semi-empirical model, like in Johnson et al. (2003), using Mars Pathfinder data, where the dust accumulation is tracked studying the discrepancy between the radio-metric calibration targets (RCT) reflectance model and the images acquired by the Imager for Mars Pathfinder (IMP) camera during the mission. Crisp et al. (2004) gives a comparison between a model not taking into account the dust accumulation and the Pathfinder observations affected by the dust deposition on the panel. The model calculates the solar irradiance at the surface and compares it to the available current, deducing the evolution of the fractional power loss along time. This fractional loss is calculated totally differently in Tanabe (2008) using a theoretical model, assuming this loss as equal to the surface coverage and considering the adsorption and desorption of airborne dust particles on solar cell surface. Finally, one of the most accurate model to describe the power attenuation of solar panels due to dust accumulation so far seems to be the empirical one described in Lorenz et al. (2020) which considers a simple attenuation factor of 0.28%/sol. To first order, this model seems to fit well with the measurements done by the solar arrays of Insight.

This paper presents a new tool that provides a good approximation of the power loss due to dust accumulation on flat or inclined surfaces, such as solar panels. This tool was included into the LMD Mars 1D thermal model, referred further as LMD1D model.

This 1D model is derived from the 3D General Circulation Model, the Mars PCM, described in Forget et al. (1999). It predicts an accurate estimation of the downward thermal infrared radiation, ground temperature, near surface air temperature and shortwave radiation on Mars. It was developed on the basis of various parametrizations of thermal and radiative processes. It uses 2-stream multiple scattering radiative transfer scheme described in Toon et al. (1989), for both the atmosphere and the accumulated dust layer.

2. Design of dust accumulation model

2.1. Dust deposition rate

To estimate the amount of dust accumulated on a surface, one must know the rate at which the dust accumulates on solar panels. The dust deposition rate R_{dust} (in kg m^{-2} s^{-1}) is computed as follows:

$$R_{\text{dust}} = mmr \times \rho_{\text{a}} \times W_{\text{s}} \tag{1}$$

with mmr the mass mixing ratio of the dust near the surface, ρ_{a} the air density and W_{s} the mean speed at which the dust falls. The latter is computed with the formula from Rossow (1978):

$$W_{\text{s}} = \frac{2}{9}\frac{\rho g}{\mu} r_{\text{sed}}^2 \left(1 + \beta \frac{4}{3} a \frac{T}{P_{\text{surf}} \times r_{\text{sed}}}\right) \tag{2}$$

* Corresponding author.
E-mail address: thomas.pierron@lmd.ipsl.fr (T. Pierron).

https://doi.org/10.1016/j.pss.2024.105985
Received 29 November 2023; Received in revised form 10 September 2024; Accepted 15 October 2024
Available online 22 October 2024

with ρ the dust density, μ the air molecular viscosity, g the acceleration of gravity, β a coefficient to take into account non-sphericity of dust particle, $a(T/P_{surf})$ the gas mean free path, $r_{sed} = r_{eff}(1 + \nu_{eff})^2$ the average particle radius for sphericity (deduced from the dust distribution effective radius r_{eff} and the effective variance of the dust size distribution ν_{eff}). All these parameters play a key role in the dust deposition, especially β and r_{eff} which significantly affect the amount of deposited dust in a given amount of time. β is the one with the most incertitude and can be tuned to fit the observations. The values for dust properties (r_{eff}, ν_{eff}) are given and discussed in Wolff et al. (2009). These parameters are set to the following values:

$$\begin{cases} \rho = 2500 \text{ kg m}^{-3} \\ \mu = 10^{-5} \text{ Pa s} \\ g = 3.72 \text{ m s}^{-2} \\ \beta = 0.5 \\ a = 1.6\ 10^{-5} \text{ m Pa K}^{-1} \\ r_{eff} = 2.0\ 10^{-6}\text{m} \\ \nu_{eff} = 0.5 \end{cases}$$

We assume that the dust is well mixed in the atmosphere. This is probably true in the Planetary Boundary Layer where the bulk of the dust loading is. Thus, we can assume that the near surface dust mass mixing ratio is a function of the column dust opacity τ of the atmosphere, the single scattering extinction coefficient at visible wavelengths $Q_{ext} = 2.4$ and the surface pressure P_{surf}:

$$mmr = \frac{4}{3}\frac{\rho r_{eff}\tau}{Q_{ext}}\frac{g}{P_{surf}} \tag{3}$$

Consequently, a good estimation of the dust opacity in the atmosphere is essential to know the amount of dust accumulated on the solar panels. This is why full dust scenarios were added to the LMD1D model. These scenarios, one for each Martian Year (MY) from MY24 to MY35 (described in Montabone et al. (2015) and Montabone et al. (2020)), are based on observations from April 1999 to today and contain daily values (over 669 sols of a Martian year) of infrared (9.3 μm) absorption column dust optical depth at 610Pa, with a horizontal resolution of 5° in longitude × 5° in latitude. This opacity is converted to the extinction optical depth in the visible (0.67 μm) and is used in Eq. (3). The conversion coefficients values are discussed in Smith (2004) and Wolff and Clancy (2003).

$$\begin{cases} \tau_{ext}(9.3\ \mu\text{m}) = 1.3 \times \tau_{abs}(9.3\ \mu\text{m}) \\ \tau_{ext}(0.67\ \mu\text{m}) = 2 \times \tau_{ext}(9.3\ \mu\text{m}) \end{cases} \tag{4}$$

At each time step, the dust deposition rate is integrated in time to calculate the total mass of dust which has been accumulated since the beginning of the run:

$$M_{dust}(t) = \int_0^t R_{dust}(t')\,dt' \tag{5}$$

2.2. Radiative transfer in the accumulated dust layer

In order to calculate the radiative transfer in the dust layer, we use the same model than the one used for the atmosphere, ie. the 2-stream multiple scattering scheme, presented in Toon et al. (1989). Once the attenuation due to the atmosphere has been calculated and the inclination of the slope has been taken into account (see Spiga and Forget (2008) for details on the method), we use the incident solar flux $\Phi_{incident}$ (in W m^{-2}) on the top of the accumulated dust layer that results from this attenuation of the atmosphere to calculate the solar flux under the dust layer Φ_{panel} (in W m^{-2}). This incident solar flux, $\Phi_{incident}$, depends on location, time, as well as the tilt angle and orientation of the slope. Kerr et al. (2023) demonstrate that this flux can be optimized at specific locations to maximize the energy received by the solar panels during one Martian year.

The model used to calculate the attenuation by the accumulated dust layer takes as inputs the single scattering albedo of dust particle ω to know the fraction of light scattered by the individual dust particles, the asymmetry parameter of the dust g_{dust} which characterizes the direction where the light will be scattered, the cosine of the solar zenith angle μ_s on the slope, the albedo of the solar panel α and the dust optical depth of the accumulated dust which has been deposited on the solar panel τ_{acc}. This last input is calculated as follows:

$$\tau_{acc} = \frac{3M_{dust}Q_{ext}}{4\rho r_{acc}} \tag{6}$$

where r_{acc} is the effective radius of the dust particles deposited on the panel, which differs from the one in the atmosphere because of the aggregation of the dust particles accumulating on the solar panel. This is a poor man's way of solving the radiative transfer through dust particles in contact on the solar panel but using the same radiative transfer model than the one used in the atmosphere for a population of aerosols. A similar model was developed by Kinch et al. (2007) to derive the dust deposition rate at the Spirit and Opportunity locations by analyzing calibration data from the PANCAM instrument of the MER mission. However, the radiative transfer model used did not account for angle-dependent parameters such as dust grain scattering functions or opposition effect parameters, and relied only on a diffusive reflectance two-layer radiative transfer model. The value of the parameter r_{acc} is studied in Landis et al. (2006) and will be discussed in the next section. The other parameters are set as follows:

$$\begin{cases} \omega = 0.8 \\ g_{dust} = 0.7 \\ \alpha = 0.25 \end{cases}$$

As mentioned above, Q_{ext} was set to 2.4 as estimated for the Martian airborne dust. The value of Q_{ext} could be different for larger aggregate of particles, and with a wide size distribution. In theory Q_{ext} could thus be closer to 2, the expected value for large particle in geometric optic. Estimating its real value is out of the scope of our study, and we can consider that varying the effective radius in Eq. (6) also account for the possible changes in Q_{ext} for the deposited dust.

The parameter μ_s is computed using the following equation:

$$\mu_s = \max[0, \mu_0\cos(\theta) + \sqrt{1-\mu_0^2}\sin(\theta)\cos(\psi - \psi_0)] \tag{7}$$

with μ_0 the cosine of the solar zenith angle, ψ_0 the solar azimuth, θ the slope inclination and ψ the slope orientation.

Then, the radiative transfer takes into account the multiple scattering and once the solar flux under the dust layer Φ_{panel}, which is really received by the surface, has been computed with all these parameters, we can calculate an attenuation coefficient (also called dust factor) $DF(t)$ in order to compare it with observation data (see next section):

$$DF(t) = \frac{\Phi_{panel}(t)}{\Phi_{incident}(t)} \tag{8}$$

The variable Φ_{panel} is the one which is provided in the outputs file over the simulation duration in the LMD1D model. Note that the solar flux received by the panel is computed over time assuming no cleaning events such as dust devils. A similar quantity, referred to as the 'Dust Correction Factor (DCF)', is derived for the Perseverance location in Vicente-Retortillo et al. (2024). However, this approach models the dust deposition in a simpler way while also taking into account dust removal with a basic term in the DCF. In our study, we do not compare our model with this DCF, but future work could explore such a comparison.

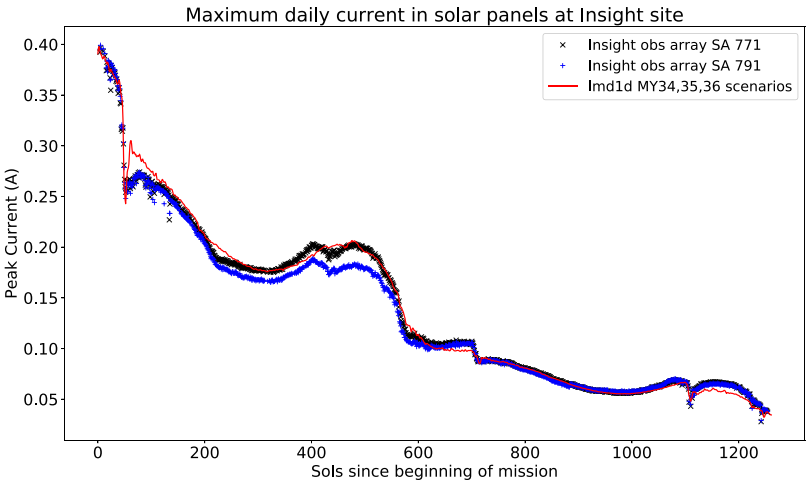

Fig. 1. Maximum daily current (in A) measured by the two solar panels (blue for SA791, black for SA771) of Insight over time (sols). The red solid line corresponds to LMD1D. *Source:* The measurements are taken from Lorenz et al. (2020).

3. Validation of the model

While the electrical current measured by the solar panels of one of the last Mars mission, Insight, is available on the Planetary Data System on NASA website, most of direct electrical data from the other missions remains unavailable. Only an estimation of the dust factor, defined in the previous section, is accessible for the Mars Exploration Rover (MER), Pathfinder and Phoenix missions. As shown in the previous section, this dust factor depends not only on the electrical current measured by the solar panel (assumed to be proportional to the solar flux Φ_{panel}) but also on the incident solar flux Φ_{incident} which cannot be measured and therefore results from an atmospheric radiative transfer model used by the mission engineering team and for which we have no details. This is why the comparison with the Insight data, which compares directly the current measured by the panels and the LMD1D model is the most relevant.

3.1. Insight

We used the LMD1D model to compare our accumulation dust model with the electrical current measured by the solar panels of the Insight mission during the first 1260 sols. To model the dust aggregation on the panel, we made the effective radius of dust particles on the panel evolve linearly with accumulated dust mass as follows:

$$r_{\text{acc}}(t) = r_{\text{acc}_{\text{init}}} + \lambda M_{\text{dust}}(t) \tag{9}$$

with $\lambda = 30$ μm kg^{-1} m^2 and $r_{\text{acc}_{\text{init}}} = 7$ μm which is about three times larger than the size of dust particles suspended in the atmosphere. These values are chosen to fit the best with the observations and will be used for comparison of the model with other missions. As said before, this can be explained by the fact that once the dust falls on the solar panel, the particles are in contact which modifies the apparent particle size compared to when particles are airborne.

To model the current, we considered it as proportional to the solar flux received by the panel with a constant proportionality factor over time. This coefficient was calculated to fit with the observations at the beginning of the mission, when there were no dust on the panel yet. Fig. 1 presents the maximum daily current measured by the Insight solar panels, ie. around noon. The slight gap around sol 60 is due to a known problem with the dust scenario which underestimates the duration of the dust storm and consequently maintains the current higher. Indeed, comparing the scenario with the dust opacity measured by Insight, we can see the real decrease of the dust opacity over time is much longer than the one in the scenario, as shown in Fig. 2.

In order to evaluate the diurnal cycle of the solar flux, we also compared the model with the Insight measurements over a few days with several values per day. This also allows to check the effect of the solar zenith angle. The comparison is shown on Fig. 3.

3.2. Spirit and opportunity

For the MER missions, only the dust factor which represents the attenuation coefficient due to accumulated dust is available to us so far. Therefore the comparison between these data and the LMD1D model is not totally consistent. Moreover, given the large duration of the MER missions, several cleaning events were observed during the missions. These cleaning events were simulated starting a new simulation after each cleaning event, with the amount of dust corresponding to the dust factor reported at this exact same date.

The Opportunity measurements are compared with the LMD1D model, setting the effective particle radius of accumulated dust according to Eq. (9). The comparison is shown on Fig. 4.

Even if the dust factor is slightly overestimated between sols 300 and 500 and underestimated between sols 1300 and 1500, we can see that the model gives a good overall fit for long term variations of the dust factor. The same comparison was done for Spirit, as shown on Fig. 5. The model for Spirit slightly underestimates the dust factor.

3.3. Pathfinder

The Pathfinder mission occurred in MY23 so there is no available dust scenario for this mission. Since the observations of the electrical current from the Pathfinder solar panels show that MY23 was a dusty year, the LMD1D model was used with the MY27 scenario which is also a year with relatively high dust optical depth. During the period of operation on Pathfinder ($L_s = 142° - 188°$), no cleaning events were observed, therefore only one simulation was done with r_{acc} following Eq. (9). The slight increases of the reported dust factor are not considered to result from cleaning events. In fact these rises can be explained by different causes: the fact that the current was not measured exactly at noon or the way the dust factor was computed from the real measurements. The comparison, shown on Fig. 6, gives a good fit overall even if locally, some gaps between the model and the measurements are observed. This can be explained by the fact that we do not use the optical depth of the atmosphere from MY23 but from another year which may differ a little.

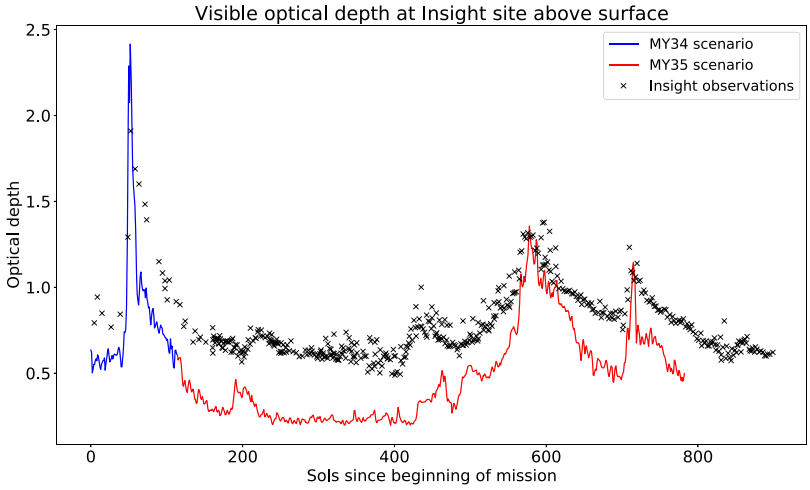

Fig. 2. Visible optical depth above surface at Insight site over time (sols). The dust storms, especially the one at the end of MY34, is shorter in the scenario than what was really measured by the Insight instrument. The discrepancy between the observed opacity by Insight and the dust scenarios is thought to result from water ice clouds. More details about this gap are given in Montabone et al. (2020). The Insight optical depth data were sourced from Spiga et al. (2018).

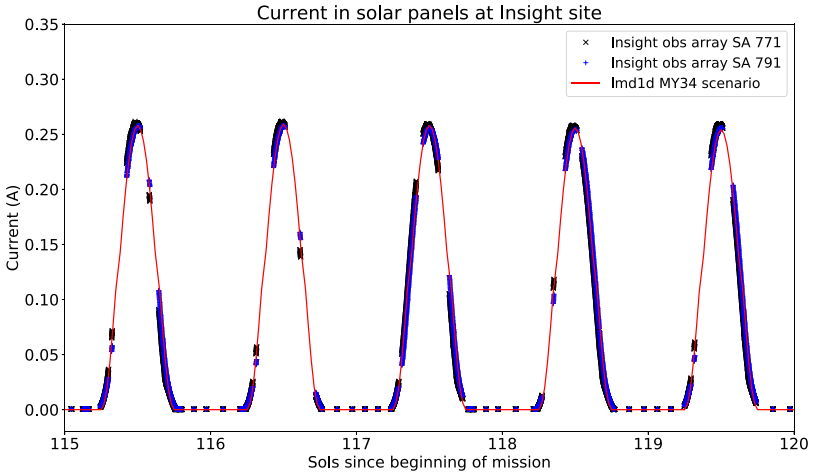

Fig. 3. Current (in A) measured by the two solar panels (blue for SA791, black for SA771) of Insight over time (sols). One can see that the current is maximum at noon and null during night.
Source: The measurements are taken from Lorenz et al. (2020).

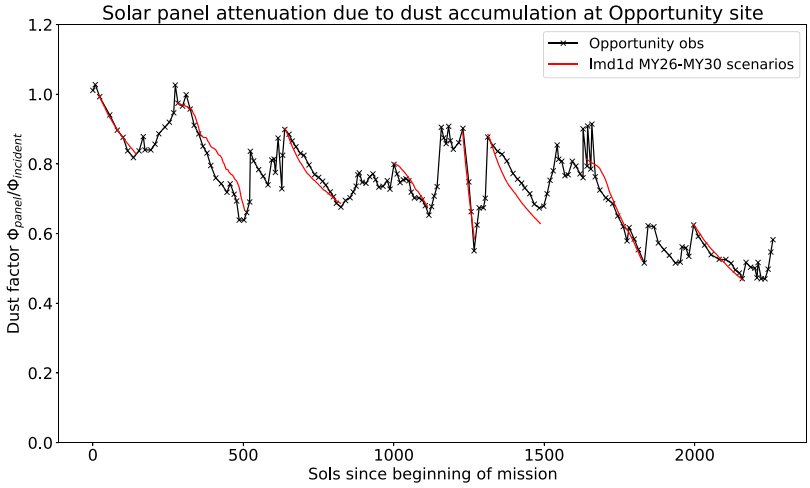

Fig. 4. Maximum daily dust factor measured by Opportunity over time (sols). The red solid line corresponds to LMD1D model with the appropriate scenarios. The measurements are taken from Stella and Herman (2010).

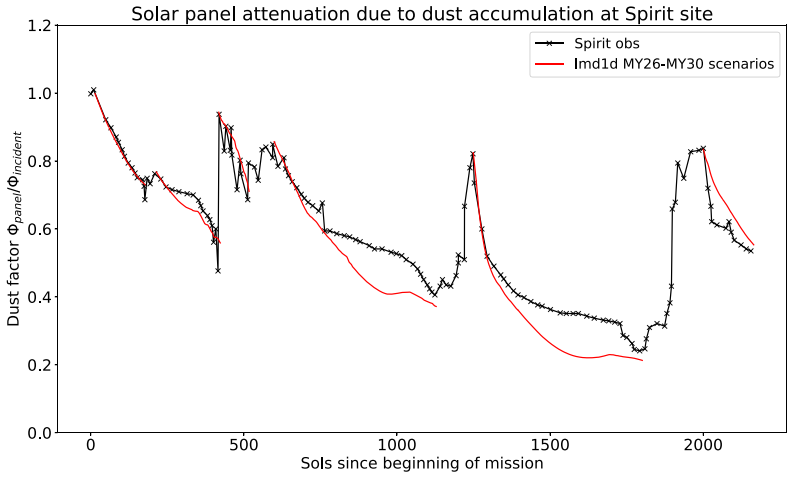

Fig. 5. Maximum daily dust factor measured by Spirit over time (sols). The red solid line corresponds to LMD1D model with the appropriate scenarios.
Source: The measurements are taken from Stella and Herman (2010).

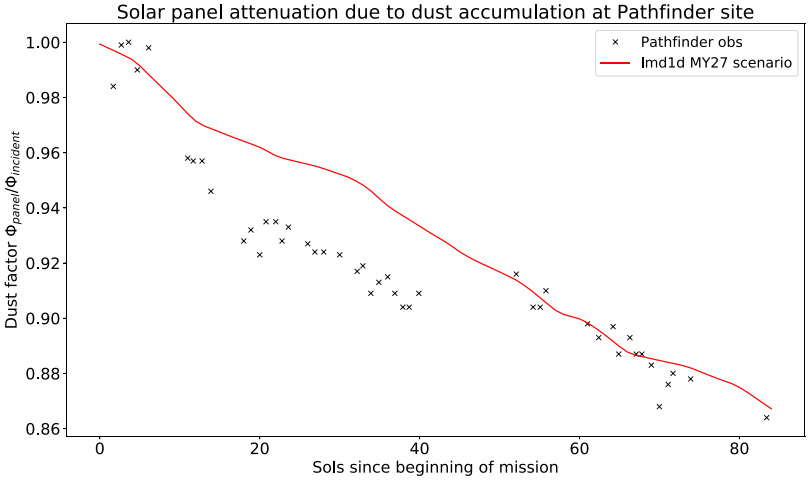

Fig. 6. Maximum daily dust factor measured by Pathfinder over time (sols). The solid line in red corresponds to LMD1D model with the MY27 scenario.
Source: The measurements are taken from Crisp et al. (2004).

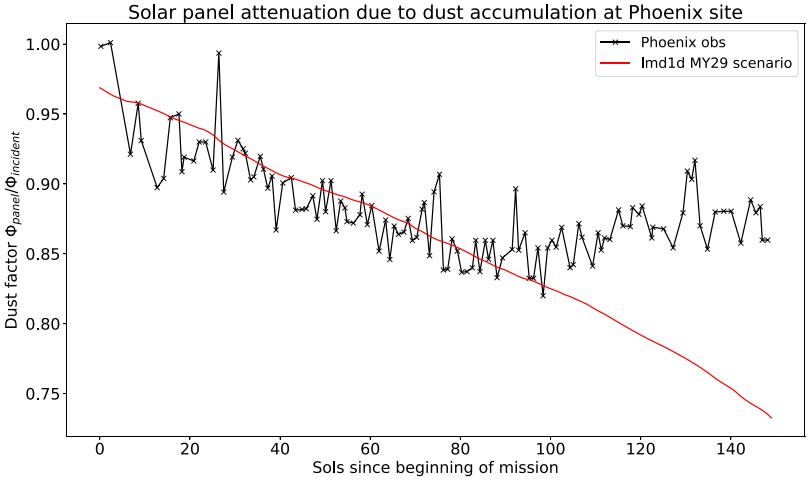

Fig. 7. Maximum daily dust factor measured by Phoenix over time (sols). The solid red line corresponds to LMD1D model with the MY29 scenario. The simulation starts with a dust factor of 0.97 to simulate the dust lifted during the landing. The solid line in black correspond to the observations done by Phoenix solar panel.
Source: The measurements are taken from Drube et al. (2010).

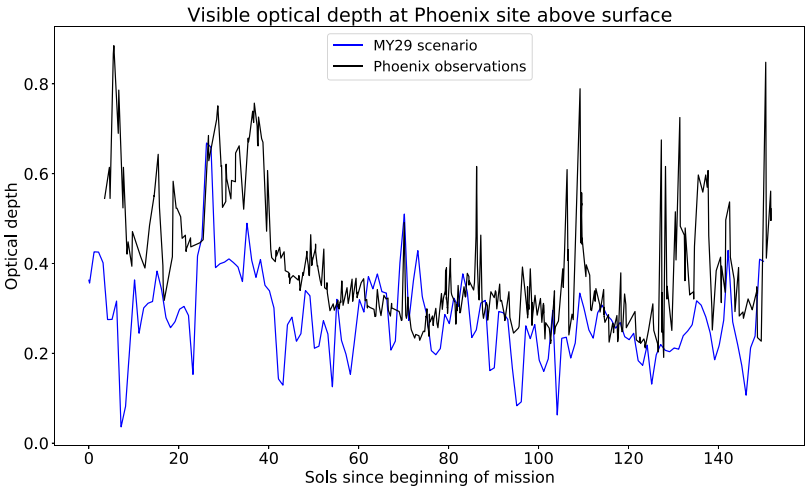

Fig. 8. Visible dust optical depth above surface over time (sols) at Phoenix site: measured by SSI (Surface Stereo Imager) in black and predicted by the MY29 scenario in blue. Dust opacity datasets are presented in Drube et al. (2010).

3.4. Phoenix

The current of the solar panels from Phoenix mission was also recorded and used to derive a dust factor which can be compared to the LMD1D model. We chose to start our simulation with a dust factor of 0.97 to simulate the large amount of dust that might have been lifted and redeposited during and after the landing, as explained in Drube et al. (2010). The effective radius r_{acc} was also set according to Eq. (9). The comparison is presented on Fig. 7. Here again no cleaning events were considered in the simulation, the slight increases before sol 100 assumed to be caused for the same reasons than Pathfinder measurements. However, after sol 100, as we can see, the dust factor increase might be explained by cleaning events. It could also be explained by the fact that the modeled current (the one that would be received without accumulated dust layer) used to calculate the dust factor was computed miscalculating the effect of the dust and clouds in the atmosphere.

Note that during the first sols of the mission, the available current in the solar cell decreases rapidly while the LMD1D dust factor is maintained high. As explained before, this is probably due to the difference between the dust opacity used in the LMD1D model and the one really measured by the "Surface Stereo Imager" (SSI) of Phoenix. The Phoenix measurements show the existence of high dust opacities in the atmosphere at the beginning of the mission obscuring the solar flux received by the panel. Drube et al. (2010) attributes this high opacity to the dust lifted during the landing. However the dust opacity in the MY29 scenario remains low as shown on Fig. 8.

4. Conclusion

Modeling the gravitational deposition of dust and the radiative effect of dust in the atmosphere and accumulated on a surface enables a good physical prediction of the surface power in W m^{-2} received by a surface such as a solar panel. Such a calculation is now included in the updated version of the LMD1D model. The inclination and the orientation of the panel are taken into account in the model and can be specified as inputs of the model. However, the model does not take into account any dust cleaning events. This makes it pessimistic and therefore, a good tool for future missions. The comparisons with the available observations are satisfying, especially the one with Insight measurements, which is the most consistent one given that it is the only one comparing directly the model with the electrical current measured by the panels. Indeed for other missions, only the dust factor, which is a semi-theoretical semi-observational data, was available. Future comparisons, especially with the MER missions electrical data that are not available yet, will be more accurate.

CRediT authorship contribution statement

Thomas Pierron: Writing – original draft, Visualization, Validation, Software, Methodology, Investigation, Formal analysis. **François Forget:** Writing – original draft, Visualization, Validation, Methodology, Investigation, Funding acquisition, Formal analysis. **Ehouarn Millour:** Writing – original draft, Visualization, Validation, Software, Methodology, Investigation, Formal analysis. **Antoine Bierjon:** Writing – original draft, Visualization, Validation, Software, Methodology, Investigation, Formal analysis.

Declaration of competing interest

The authors declare that they have no known competing financial interests or personal relationships that could have appeared to influence the work reported in this paper.

Acknowledgments

This project has received funding from the European Space Agency, CNES and the European Research Council (ERC) under the European Union's Horizon 2020 research and innovation programme (grant agreement No 835275, project "Mars Through Time").

Data availability

Data will be made available on request.

References

Crisp, D., Pathare, A., Ewell, R., 2004. The performance of gallium arsenide/germanium solar cells at the Martian surface. Acta Astronaut. 54 (2), 83–101.

Drube, L., Leer, K., Goetz, W., Gunnlaugsson, H.P., Haspang, M.P., Lauritsen, N., Madsen, M., Sø rensen, L., Ellehoj, M., Lemmon, M., et al., 2010. Magnetic and optical properties of airborne dust and settling rates of dust at the phoenix landing site. J. Geophys. Res.: Planets 115 (E5).

Forget, F., Hourdin, F., Fournier, R., Hourdin, C., Talagrand, O., Collins, M., Lewis, S.R., Read, P.L., Huot, J.-P., 1999. Improved general circulation models of the Martian atmosphere from the surface to above 80 km. J. Geophys. Res.: Planets 104 (E10), 24155–24175.

Johnson, J.R., Grundy, W.M., Lemmon, M.T., 2003. Dust deposition at the mars pathfinder landing site: Observations and modeling of visible/near-infrared spectra. Icarus 163 (2), 330–346.

Kerr, J., Moores, J.E., Smith, C.L., 2023. An improved model for available solar energy on mars: Optimizing solar panel orientation to assess potential spacecraft landing sites. Adv. Space Res. 72 (4), 1431–1447.

Kinch, K.M., Sohl-Dickstein, J., Bell III, J.F., Johnson, J.R., Goetz, W., Landis, G.A., 2007. Dust deposition on the mars exploration rover panoramic camera (pancam) calibration targets. J. Geophys. Res.: Planets 112 (E6).

Landis, G.A., 1996. Dust obscuration of mars solar arrays. Acta Astronaut. 38 (11), 885–891.

Landis, G., Herkenhoff, K., Greeley, R., Thompson, S., Whelley, P., et al., 2006. Dust and sand deposition on the MER solar arrays as viewed by the microscopic imager. LPI 1932.

Landis, G.A., Jenkins, P.P., 2000. Measurement of the settling rate of atmospheric dust on mars by the MAE instrument on mars pathfinder. J. Geophys. Res.: Planets 105 (E1), 1855–1857.

Lorenz, R.D., Lemmon, M.T., Maki, J., Banfield, D., Spiga, A., Charalambous, C., Barrett, E., Herman, J.A., White, B.T., Pasco, S., et al., 2020. Scientific observations with the InSight solar arrays: Dust, clouds, and eclipses on mars. Earth Space Sci. 7 (5), e2019EA000992.

Montabone, L., Forget, F., Millour, E., Wilson, R., Lewis, S., Cantor, B., Kass, D., Kleinböhl, A., Lemmon, M., Smith, M., et al., 2015. Eight-year climatology of dust optical depth on mars. Icarus 251, 65–95.

Montabone, L., Spiga, A., Kass, D.M., Kleinböhl, A., Forget, F., Millour, E., 2020. Martian year 34 column dust climatology from mars climate sounder observations: Reconstructed maps and model simulations. J. Geophys. Res.: Planets e2019JE006111.

Rossow, W.B., 1978. Cloud microphysics: Analysis of the clouds of earth, venus, mars and jupiter. icarus 36 (1), 1–50.

Smith, M.D., 2004. Interannual variability in TES atmospheric observations of mars during 1999–2003. Icarus 167 (1), 148–165.

Spiga, A., Banfield, D., Teanby, N.A., Forget, F., Lucas, A., Kenda, B., Rodriguez Manfredi, J.A., Widmer-Schnidrig, R., Murdoch, N., Lemmon, M.T., et al., 2018. Atmospheric science with insight. Space Sci. Rev. 214, 1–64.

Spiga, A., Forget, F., 2008. Fast and accurate estimation of solar irradiance on Martian slopes. Geophys. Res. Lett. 35 (15).

Stella, P.M., Herman, J.A., 2010. The mars surface environment and solar array performance. In: 2010 35th IEEE Photovoltaic Specialists Conference. IEEE, pp. 002631–002635.

Tanabe, K., 2008. Modeling of airborne dust accumulation on solar cells at the Martian surface. Acta Astronaut. 62 (12), 683–685.

Toon, O.B., McKay, C., Ackerman, T., Santhanam, K., 1989. Rapid calculation of radiative heating rates and photodissociation rates in inhomogeneous multiple scattering atmospheres. J. Geophys. Res.: Atmos. 94 (D13), 16287–16301.

Vicente-Retortillo, A., Lemmon, M., Martinez, G., Toledo, D., Apéstigue, V., Arruego, I., Bertrand, T., Lorenz, R., Sebastián, E., Hueso, R., et al., 2024. Dust accumulation and lifting at the landing site of the mars 2020 mission, Jezero crater, as observed from MEDA. Geophys. Res. Lett. 51 (11), e2023GL107975.

Wolff, M.J., Clancy, R.T., 2003. Constraints on the size of Martian aerosols from thermal emission spectrometer observations. J. Geophys. Res.: Planets 108 (E9).

Wolff, M., Smith, M., Clancy, R., Arvidson, R., Kahre, M., Seelos, F., Murchie, S., Savijärvi, H., 2009. Wavelength dependence of dust aerosol single scattering albedo as observed by the compact reconnaissance imaging spectrometer. J. Geophys. Res.: Planets 114 (E2).